

RADIUS INFLATION AT LOW ROSSBY NUMBER IN THE HYADES CLUSTER

KARL JAEHNIG^{1,2}, GARRETT SOMERS^{2,3}, AND KEIVAN G. STASSUN^{2,1}

¹Department of Physics, Fisk University, Nashville, TN, 37208, USA

²Department of Physics and Astronomy, Vanderbilt University, Nashville, TN 37235, USA

³Vanderbilt Initiative in Data-intensive Astrophysics Fellow

ABSTRACT

Radius inflation continues to be explored as a peculiar occurrence among magnetically active, low-mass stars. Recently Somers & Stassun (2017) showed that radius inflation among low-mass stars in the young open cluster M45 (Pleiades Cluster) is correlated to the rotation rate: faster rotators are more inflated. Here we extend that work to a sample of 68 stars of the older open Hyades Cluster. We derive the stars’ spectral energy distributions to measure their bolometric fluxes. With spectroscopically defined T_{eff} and *Gaia* distances we calculate stellar radii using the Stefan-Boltzmann relation. We find numerous stars that exhibit significant ($3\text{--}4\sigma$) radius inflation relative to a nominal cluster isochrone. We compare these results to that of the younger Pleiades and consider radius inflation as a function of open cluster evolution. We find that unlike the Pleiades, there is not a statistically significant correlation between radius inflation and stellar rotation period. However, we do find that most inflated stars have (rapid) rotational Rossby numbers of 0.1–0.2, such that the correlation of radius inflation with Rossby number is statistically significant at 99.98% confidence. Because the canonical rotation-activity relation of low-mass stars is understood to result from the connection between magnetic activity and surface convection, our results imply that magnetic activity within the convective layers of low-mass stars is what preferentially drives radius inflation.

Keywords: Astrophysics - Solar and Stellar Astrophysics

1. INTRODUCTION

A consensus is emerging that some low-mass stars ($M \lesssim 1M_{\odot}$) have larger radii than expected from standard stellar theory. This so-called “radius inflation” effect is typically of order 10–15% and is correlated with a roughly 5–10% lower effective temperature than predicted. Radius inflation has been observed in numerous studies using a variety of observational techniques including eclipsing binary analysis (e.g. Popper 1997; Torres & Ribas 2002; López-Morales & Ribas 2005), statistical projected radii (e.g. Jackson et al. 2016, 2018), and spectral energy distributions (SEDs) (Somers & Stassun 2017, S2017 hereafter). Though the precise mechanism is still debated, strong magnetic activity seems to play a role either through the direct inhibition of convective energy transport, the influence of large starspots on the photospheric pressure and temperature, or a combination of both effects (e.g. Mullan & MacDonald 2001; Chabrier, Gallardo & Baraffe 2007; Macdonald & Mullan 2010; Feiden & Chaboyer 2013, 2014; Jackson & Jeffries 2014a,b; Somers & Pinsonneault 2014, 2015b,a). This conclusion is based on observed correlations between radius inflation and proxies of magnetic activity such as $H\alpha$ emission, X-rays, and rotation rate (e.g. López-Morales & Ribas 2005; Stassun et al. 2012; Somers & Stassun 2017).

S2017 investigated whether any of the single K-dwarfs in the young Pleiades open cluster showed evidence of radius inflation. By measuring the SEDs of the stars to determine their luminosities, measuring their effective temperature using color proxies, and solving the Stefan-Boltzmann equation, S2017 determined the radii of 80+ Pleiads and compared them to stellar evolution models. They found that for stars rotating with a period slower than 2 d, corresponding to a Rossby number¹ (R_N) greater than ~ 0.1 in the mass range they studied ($\sim 0.7 - 0.9M_{\odot}$), the models predicted the T_{eff} -radius relation extremely well. However, stars rotating faster than 2 d ($R_N \lesssim 0.1$) were on average $\sim 12\%$ larger than predicted. This is an interesting value of R_N , as numerous other studies have found that the correlation between rotation rate and magnetic proxies saturates at approximately this value (e.g. Wright et al. 2011). This suggests that the radius inflation mechanism may be connected to the as-yet unclear physics of magnetic saturation. Moreover, these inflated Pleiads tended to show higher lithium abundances as expected from stars experiencing radius inflation during their early lives (e.g. Somers & Pinsonneault 2014, 2015b,a).

Following the results of S2017, we now wish to explore the evolution of radius inflation with stellar age. If radius inflation is a consequence of magnetic activity and rapid rotation,

karl.o.jaehnig@vanderbilt.edu

¹ The Rossby number is defined as the ratio of the rotation period to the convective overturn timescale (e.g. Noyes et al. 1984).

it stands to reason that the degree of radius inflation at fixed spectral type should decline with increasing age as stars both spin down and become less magnetically active (e.g. [Skumanich 1972](#)). If in fact radius inflation exists for stars with Rossby numbers below ~ 0.1 as suggested by the results of [S2017](#), then the masses of inflated stars should be lower on average in older clusters, owing to the slower spin down rate of less massive stars. As a complement to the Pleiades, this paper will focus on the Hyades.

The structure of the paper is as follows: In section 2 we discuss the data we collected to form a complete sample of the Hyades pre-main sequence stars as well as any relevant data quality measures that were employed. In section 3 we detail how we calculated the radius inflation for each star in the Hyades. In section 4 we present the results we found between the derived radii inflation within the Hyades and stellar rotation of the stars. In section 5 we discuss the implications of our results with respect to stellar evolution and with regard to previous work in radii inflation. We present a summary of our findings in section 6

2. DATA

2.1. The Hyades sample

In order to properly derive effective temperatures for the stars within the Hyades, it is necessary to build a sample of known members and their magnitude measurements in different bands. We start with the Hyades membership list from the [Goldman et al. \(2013, G2013 hereafter\)](#) catalog. [G2013](#) made use of Pan-STARRS ([Chambers et al. 2016](#)) and PPMXL ([Roeser et al. 2010](#)) photometry, complimented by photometry from 2MASS ([Skrutskie et al. 2006](#)), SDSS-III DR8 ([Aihara et al. 2011](#)), and UKIDSS DR8 ([Lawrence et al. 2007](#)), in order to construct a complete stellar mass function. The [G2013](#) final sample size of Hyades member stars was 774. The [G2013](#) catalog did not have rotational periods for its final sample of Hyades stars and so it is necessary to complement the [G2013](#) photometry with other catalogues which included rotation measurements.

To this end we employ two catalogues which have Hyades member stars with measured rotational periods. [Douglas et al. \(2016, D2016 hereafter\)](#) measured rotation periods for 65 Hyades stars using the Kepler spacecraft during its K2 phase in order to study low-mass star gyrochronology. We cross-matched the sample compiled by [D2016](#) against the 2MASS catalog in order to find complimentary stars within the membership catalog from [G2013](#). We find that all 65 of the [D2016](#) Hyades stars have cross-matches within the [G2013](#) catalog.

[Delorme et al. \(2011, D2011 hereafter\)](#) also measured rotation periods for 63 Hyades stars in order to also study gyrochronology within the Hyades. We cross matched the catalog from [D2011](#) with the catalog from [G2013](#) and find 59 Hyades stars with period-of-rotation measurements. Within this set of 122 stars we checked for stars with double observations, finding 13 stars that have observations in both [D2011](#) and [D2016](#), thus reducing our initial sample to 109 stars with individual period-of-rotation measurements. For Hyades stars with double observations, we employed the period-of-rotation measurements from the more recent [D2016](#)

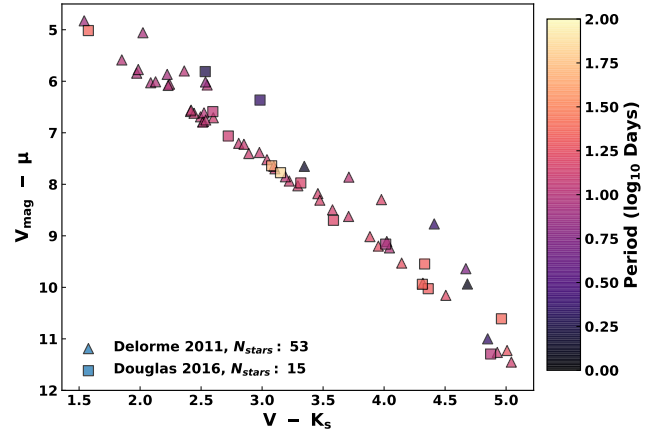


Figure 1. Color-magnitude diagram of the Hyades sample used in this work. Triangles are sources taken from [Delorme et al. \(2011\)](#) and squares are sources taken from [Douglas et al. \(2016\)](#). The points are all colored by their period in \log_{10} days.

catalog. We plot the color-magnitude diagram of this sample in Figure 1.

Having compiled a set of Hyades members with measured periods, we moved to collect photometry in order to calculate the T_{eff} . We queried the SIMBAD database ([Wenger et al. 2000](#)) in order to gather photometry in the Johnson passbands ($UBVR_J I_J JHK$). We found that there is sufficient V and K_S 2MASS photometry to calculate T_{eff} using the $V - K_S$ color. We cross-matched 2MASS IDs with CDS to download the K_S magnitudes and use the V magnitudes from [Johnson & Knuckles \(1955\)](#) in order to assemble our sample of colors for the Hyades stars.

With these data we assembled our initial sample of 109 Hyades stars with $V - K_S$ photometry, and measured rotation periods. In section 3.2 we go into detail on deriving T_{eff} values for our initial sample which pruned our initial sample size of 109 stars to 68 due to constraints on applicable color range for the derived color- T_{eff} polynomial fits. In section 3.3 we detail our search of the previous literature for confirmed spectroscopic/visual binaries within our Hyades sample, finding 23 binaries within our sample of 68 Hyades stars. Our **final sample** of Hyades stars consists of this group of 45 confirmed single stars and 23 identified binaries. We provide the 2MASS IDs, positions, photometric measurements, and measured rotation period for these 68 Hyades stars in Table 1.

3. METHODS

3.1. Overview

The constraints applied to the data that we have just described largely follow the same conventions employed by [S2017](#) in their analysis of the Pleiades cluster. In the following sections we outline our methods in analyzing our sample of Hyads. We also introduce a novel method for calculating stellar radius inflation that takes into account the relationship between T_{eff} and radius (see section 3.6).

We aim to compare our results to the Pleiades results from [S2017](#), but their method for determining ΔR did not account for this relationship. Instead, they simply used the isochronal radius at the measured T_{eff} of the star as a comparison point.

A direct comparison with their values would therefore be biased. Instead, we recompute radius inflation for the Pleiades using the methods we have developed in section 3.6.

Using the well known Stefan-Boltzmann law

$$L = 4\pi R_*^2 \sigma_{\text{SB}} T_{\text{eff}}^4, \quad (1)$$

the radius of a star can be derived if its luminosity and T_{eff} are known with acceptable precision. The luminosity can be determined using the equation

$$L = 4\pi d^2 f_{\text{bol}}, \quad (2)$$

where f_{bol} is the bolometric flux and d is the distance to the star. The T_{eff} calculation remains the most crucial task in studying radius inflation, as it is the biggest contributor to the final uncertainty in the calculated radius ($R \propto L^{1/2} T^{-2}$). In the subsections that follow, we briefly go over the derivation of T_{eff} , the bolometric flux f_{bol} , and the stellar radii for our sample of Hyads. The methods used in the derivations of T_{eff} , and f_{bol} are the same used in S2017.

3.2. Effective Temperature

In order to calculate T_{eff} using the $V - K_S$ color we need to account for any possible extinction present in the Hyades. Since the Hyades is both within the local bubble and an older open cluster (650 ± 70 Myr, from Martín et al. 2018), there is very little extinction arising within the cluster or in the intervening ISM. We adopt $E(B - V) = 0.01$ (Gunn & Stryker 1983), a typical value quoted for the Hyades. To convert this value to other colors, we employ the standard reddening law from Cardelli et al. (1989) with a selective reddening of $R_V = 3.1$. This gives us an $E(V - K_S)$ value of 0.027 ± 0.01 . With this we then proceed to use the empirical metallicity dependent calibrations from Huang et al. (2015) to calculate T_{eff} using $V - K$, adopting $[\text{Fe}/\text{H}] = 0.13 \pm 0.01$ (Paulson et al. 2003). These color- T_{eff} calibrations are valid over a $V - K_S$ color range of [0.85, 5.05].

We propagated the uncertainties on our $V - K_S$ color, the extinction $E(V - K_S)$ quoted for the Hyades, and the Hyades metallicity $[\text{Fe}/\text{H}]$ to get our overall uncertainties on T_{eff} . These individual uncertainties on T_{eff} are in the range of 5–34 K. We also had a systematic spectroscopic uncertainty of 60 K calculated from the polynomial fits of Huang et al. (2015). Our overall T_{eff} uncertainty ranges over 65–94 K.

3.3. Accounting for Binaries within our Hyades Sample

When it comes to the study of radius inflation in single stars, binaries pose a problem, as they can produce false indications of radius inflation photometrically. This problem arises from the additional flux from an unresolved binary system, causing observations to result in a higher measured magnitude. Typically, photometric binaries are identified because they form their own main sequence above the single star main sequence in the color-magnitude diagram. This effect has already been explored by S2017 who searched for and excluded binaries within their Pleiades sample. We summarize their conclusions of the effects of binaries on radii inflation below:

- Equal mass binaries will increase bolometric flux without significantly affecting the measured T_{eff} , thus leading to a significant signal of radius inflation
- For low-mass-ratio binaries, the total bolometric flux is barely affected but the near-IR emission is significantly boosted, leading to a lower inferred T_{eff} calculation. This can result in a false signal of radius inflation because the lower inferred temperatures means the star will be compared to the radius predicted for a lower-mass star.

We proceeded to look through our sample of Hyades stars for binary systems that have been confirmed with previous surveys. We focused primarily on finding confirmation either through spectroscopic surveys, which involve measuring the radial velocity and possible calculation of the orbital elements, or optical surveys, where the binary is resolved and its motions can be calculated.

As the Hyades is among the most observed open clusters, it was not difficult to find several surveys that considered both cluster membership and binarity. For our sample of Hyades stars we consulted Kopytova et al. (2016) for an initial list of their identified single stars, as well as the works they used to exclude stars that were in binary systems. We constructed a list of confirmed multiple systems using the catalogs of Mermilliod, Mayor & Udry (2009), Patience et al. (1998), and Duchêne et al. (2013). With this compiled list of catalogs we found that 45 stars within our sample of 68 Hyades stars had been previously identified as single stars.

For the other 23 stars within our sample we queried Vizier for any catalogues in which the binary status had been confirmed visually or spectroscopically. We found that 20 of our 23 Hyades stars are confirmed binaries, with observations coming from the Tycho Double Star Catalog (Fabricius, Høg, Makarov, Mason, Wycoff & Urban 2002), the Washington Double Star Catalog (Mason, Wycoff, Hartkopf, Douglass & Worley 2001; Douglas, et al. 2014). We could not find confirmation of binarity, or single star status for three stars and decided to exclude them from our analysis. The final binary status for our final sample can be found in the last column of Table 1, where

- No = Confirmed Single Star
- Yes = Confirmed Binary System
- Yes? = Unconfirmed Binary/Single Star.

3.4. Bolometric Flux

In order to calculate the total bolometric flux of a star, f_{bol} , we interpolated the observed spectral energy distribution (SED) of each Hyades star with a standard stellar atmosphere model from the model grid of Kurucz (2013). This is the same SED interpolation procedure employed in Stassun & Torres (2016) and was used in S2017. Note that, as described by Stassun & Torres (2016), the f_{bol} determined via this interpolation procedure is virtually independent of T_{eff} .

We adopted the Hyades metallicity and the T_{eff} derived in Section 3.2. The multiple photometric observations were col-

lected by querying *Vizier* and cover a wide wavelength spectrum from the far-ultraviolet at $\sim 0.15\mu\text{m}$ to the far-infrared at $\sim 22\mu\text{m}$. The complete list of surveys queried can be found in Section 2.3.1 of S2017. With these collected photometric observations spanning a wide wavelength spectrum it was then possible to construct an SED to calculate the total f_{bol} . The resulting SEDs have a goodness-of-fit, χ^2_{ν} , determined by comparing the observed fluxes to the passband-integrated model fluxes, and where the only free parameters in the fit are the reddening (limited to the allowable range determined above) and the overall flux normalization. These values are listed in Table 2, along with the calculated bolometric flux.

3.5. Stellar Radius

The angular radius can be derived using a rearranged version of the Stefan-Boltzmann law, accomplished by replacing the luminosity in equation 1 with the luminosity-flux relation given in equation 2. The resulting equation can be rearranged such that we get

$$\Theta = f_{\text{bol}}^{0.5} \sigma_{\text{SB}}^{-0.5} T_{\text{eff}}^{-2} \quad (3)$$

where Θ is the angular radius, given by R_*/d . As we have already calculated the total bolometric flux, as well as the T_{eff} , we can simply calculate the angular radius for our Hyades Sample by inserting these values into equation 3. We list the resulting angular radii in units of milli-arcseconds in Table 2.

Our calculated angular radii for our identified single stars have a range of [35-100] μas with an average error on the calculated angular radius of $\sim 2.5 \mu\text{as}$. Overall, the small magnitude of the angular radius error, along with the relatively small values of χ^2_{ν} indicate that the SED fits were accurate.

To get the stellar radius from the angular radius, we multiplied the angular radius Θ of a star by its distance from us. The distance to the Hyades has been found to be about 46.75 ± 0.46 pc, using TGAS data from *Gaia* Data Release 1 (Gaia Collaboration, et al. 2017). S2017 employed a single star cluster distance measurement for the Pleiades to convert their angular radii derivations to stellar radii, with an uncertainty added to the distance to reflect the depth of the Pleiades cluster.

With the recent release of *Gaia* Data Release 2 (Gaia Collaboration et al. 2018), we now have individual parallax measurements with very high precision ($\sigma_{\pi} \sim 10^{-4}$ arcsec) for our entire Hyades sample. Instead of simply inverting the *Gaia* DR2 parallaxes to derive distances, we employed the distances calculated by Bailer-Jones et al. (2018) using Bayesian Inference for our individual Hyades stars. We then derived the observed stellar radii by multiplying our individual angular radii values by the associated individual distances we have for the Hyades stars. We list these stellar radii values in units of R_{\odot} in Table 2.

The stellar radii are calculated using three other parameters, each with their associated uncertainties. These parameters are the derived T_{eff} , the total bolometric flux, and the distances for each star. We fitted a gaussian kernel density estimator to the distributions of fractional errors for the three aforementioned parameters and plot the resulting probability

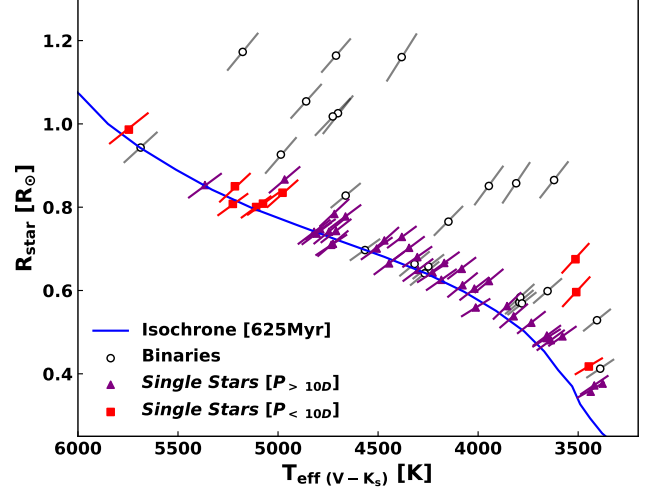


Figure 2. Calculated stellar radii for the Hyades stars against their calculated T_{eff} values. The diagonal error bars are the correlated errors between the stellar radius and the T_{eff} . The red squares are stars with measured rotation periods less than 10 day. The purple triangles are stars with measured rotation periods greater than 10 days. The empty gray circles are the identified binaries within the sample. The solid blue line is the isochrone with a cluster age of 625 Myr.

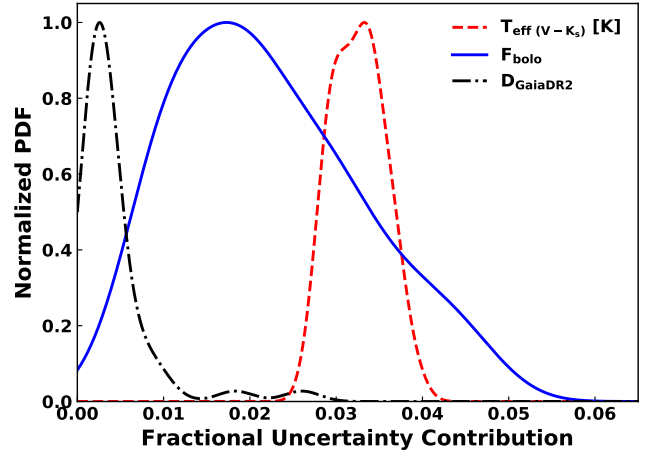


Figure 3. Normalized probability distribution functions of the fractional uncertainties that f_{bol} , T_{eff} , and Distances from *Gaia* DR2 that contribute to the error on the calculated stellar radius. These PDFs have been generated from Kernel Density estimators that were fitted to the distributions for the final sample of single stars. Here we see that the typical contributions to the uncertainty on R_* are $\lesssim 1\%$, $\lesssim 4\%$, and $\lesssim 3\%$, for distance, T_{eff} , and f_{bol} , respectively.

density functions in Figure 3. From Figure 3 it is apparent that the error in Θ and by extension, ΔR_* , is dominated by the error on T_{eff} , though can be dominated by the error on f_{bol} in some cases; the error contribution from the *Gaia* parallax is negligible in all cases.

3.6. Calculating Radius Inflation

In order to determine if a star has a larger radius than expected, we compared our derived values to stellar isochrones from the literature. Isochrones are frequently used to pre-

dict theoretical properties of stellar populations under the assumption that they are all the same age and composition. In modeling the Hyades, we decided to use isochrones generated by Somers & Pinsonneault (2014) with a cluster age of 625 Myr and a metallicity of $[Fe/H] = 0.13$. We plot this isochrone alongside our Hyades sample in Figure 2.

The method employed in calculating R_{iso} for the Pleiades in S2017 (see their section 3.3) is summarized here. Calculating the amount of radius inflation occurring with a particular star requires the measured stellar radius and the expected stellar radius based on T_{eff} from a representative isochrone. To calculate the isochronal stellar radius, R_{iso} , a spline was fitted to the isochrone relating radius and T_{eff} . Then R_{iso} is calculated for a particular star by using the fitted spline to calculate the radius at its calculated T_{eff} .

We introduced a new method for calculating the expected stellar radius R_{iso} for a star at a measured T_{eff} . As we assume that the luminosity will remain the same whether or not a star is undergoing radius inflation, we took advantage of this by calculating the luminosity, as given by equation 1 of our Hyades stars using R_* and T_{eff} .

We fit a univariate spline to the isochrone radius and luminosity from the 625 Myr isochrone. With this spline, we can then calculate R_{iso} for each of our Hyades stars. We can now proceed in calculating the radius inflation that might be taking place within the Hyades. We employ the same equation from S2017, which is written as:

$$\Delta R_* = \frac{R_* - R_{iso}}{R_{iso}} \quad (4)$$

Where R_* is the measured stellar radius we derived in section 3.5 and R_{iso} is the radius we calculated using isochrones and the calibrated T_{eff} . Thus the ΔR_* value can be more simply stated as the fractional height above the fitted isochrone.

4. RESULTS

We list the calculated overall radius inflation, ΔR , for each star within our final sample in table 2. We also re-plot the color-magnitude diagram of the Hyades within Figure 4 to include the radius inflation information. Confirmed single stars within our sample are colored by the χ^2_v values of the fitted SED and sized according to the calculated radius of inflation, using equation 4. Confirmed binary stars within the Hyades are plotted as red x's and not sized according to their degree of radii inflation. S2017 showed how their properties affect the calculation of radius inflation, causing false signals of radius inflation. Within Figure 4 we see the presence of the binary main-sequence, as well as the location of two inflated single stars within this binary main-sequence. Single stars that have undergone radius inflation are thought to exist within what is considered the binary main-sequence and are incorrectly classified as photometric binaries. We will comment on this further with respect to our results in section 5.

4.1. Relationship to Rotation Period

As mentioned in §1, radius inflation may be connected to rapid rotation. We therefore considered the connection between radius inflation and stellar rotation, as was considered

within the younger Pleiades open cluster in S2017, by looking at the observed rotation period of our Hyades sample and the radius inflation. In Figure 5 (left panel), we plot the observed rotation periods of our single stars against their calculated percentage of radii inflation. Overall we found that our Hyades sample periods are clustered around 10–15 days.

We binned the Hyades stars into two bin: the slow rotating stars (period > 10 days) and the fast rotating stars (period < 10 days). Within these two bins we found the average percentage of radius inflation and plot the two average values as the orange squares within Figure 5 (left panel).

We explored the degree of monotonicity between radius inflation and rotation period by calculating the Spearman's Rank correlation coefficient, denoted by $\rho_{spearman}$ and the Kendall Tau correlation coefficient, denoted by $\tau_{kendall}$. These coefficients describe the degree of correlation between two variables, where a value of 0 is no correlation, values >0 are positive correlations, and values < 0 are negative correlations. In addition to the actual correlation coefficient, we calculated their p-values, to test against the null-hypothesis that these correlations could be due to random chance.

For period and ΔR , we calculate a value of $\rho_{spearman} = -0.032$ and $\tau_{kendall} = -0.022$, with p-values of 0.832 and 0.829, respectively. This suggests that there is little to no correlation between period and radius inflation within this sample.

This result suggests that the relation between rotation and radius inflation found by S2017 becomes undetectable via observed rotation periods or disappears as the cluster ages and the star's magnetic fields become less active due to age related spin-down. To explore the likelihood of the second possibility, we considered also the Rossby number (Noyes et al. 1984) of the stars within the Hyades sample.

4.2. Relationship to Rossby Number

The Rossby number (R_N) is the ratio of the rotation period of a star over the convective zone overturn time, denoted by τ_{cz} , which is a timescale to describe how long it takes convective motions to traverse the convective envelope. Noyes et al. (1984) argued that the Rossby number is the preferential metric to study magnetic activity because it appears to correlate with magnetic proxies such as Ca II emission more strongly than just rotation itself.

In order to calculate the Rossby number for our Hyades sample, we employed the empirically calculated relationship between T_{eff} and the convective overturn time, τ_{cz} from Wright et al. (2011). We fitted a cubic spline to this empirical relationship and calculated the expected convective overturn rate for our Hyades sample, using their individual T_{eff} from section 3.2. We calculated the Rossby number for our Hyades sample by dividing the rotation period of our stars by their calculated τ_{cz} value.

We plot the Hyades Rossby numbers against the calculated percentage of radius inflation in Figure 5 (right panel). We bin this sample by either being slowly convective ($R_0 > .25$) or rapidly convective ($R_0 < .25$). We see there there is a greater spread in the distribution of Rossby numbers within the Hyades sample than with period, indicative of the fact

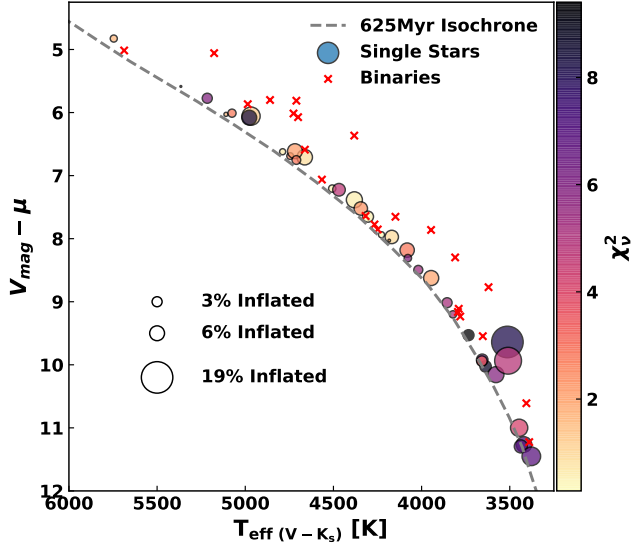


Figure 4. Temperature-magnitude diagram of the Hyades sample. The points are sized proportionally to their calculated $\Delta R_*/R_*$ and colored according to the χ^2 values for their SED fits. The gray dashed line is a 625Myr isochrone from an atmospheric model from Somers et al. 2019 (in preparation).

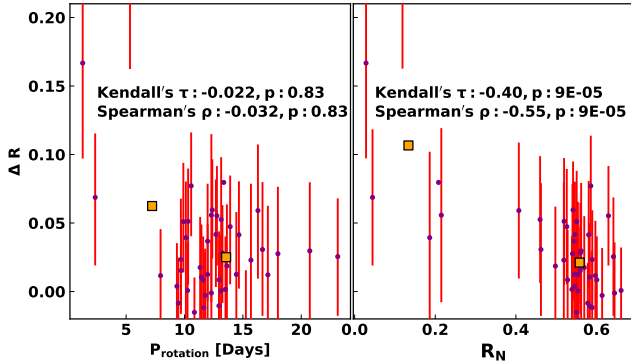


Figure 5. Left Panel: Measured rotation period of the single stars in the Hyades final sample against the calculated percentage of radius inflation from Section 3.6. The purple points are the confirmed single stars. The orange squares are the average of the sample, binned into slow rotators ($P_{\text{rot}} > 10$ d) and fast rotators ($P_{\text{rot}} < 10$ d). Right Panel: Same as left panel but with the calculated Rossby number (R_N) on the x-axis. The orange squares are the average of the sample, binned into slowly convective ($R_N > 0.25$) and rapidly convective ($R_N < 0.25$).

that most of the rapidly spinning stars are lower mass. We calculated the ρ_{spearman} and τ_{kendall} coefficients and attain values of -0.549 and -0.404 , respectively. The associated p-value are both ~ 0.0001 . This indicates that there is significantly non-random negative trend between the Rossby number and the percentage of radius inflation.

5. DISCUSSION

We have employed several measures to ensure that our data are free of spurious values and that the relationship we have found between radius inflation and rotational period is not random. In the following section we discuss possible sources

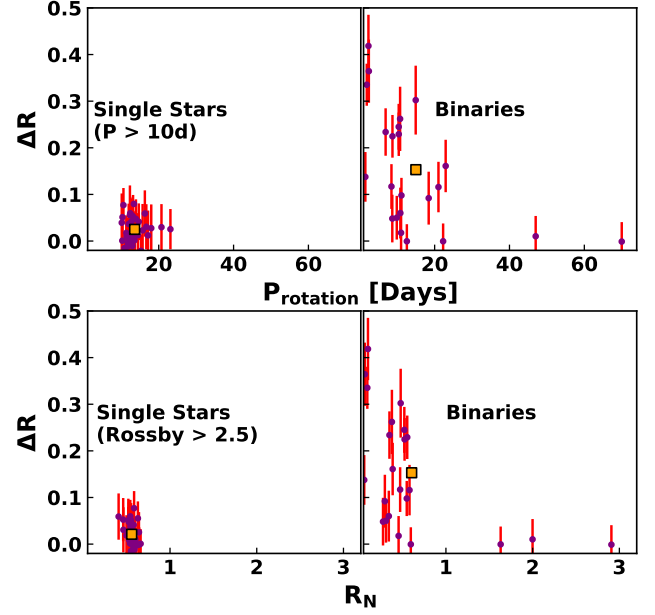


Figure 6. Top Row: ΔR versus rotation period for slowly rotating single Hyades stars (left panel) and the confirmed binary stars (right panel). Bottom Row: ΔR versus Rossby number (R_N) for “slowly convective” ($R_N > 0.25$) single stars (left panel) and the confirmed binary stars (right panel). The orange square in each panel is the average of the plotted sample.

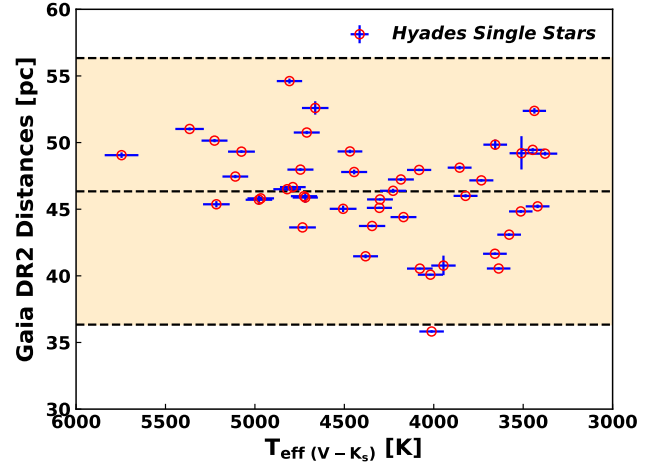


Figure 7. Inferred distances from *Gaia* DR2 parallaxes (see [Bailer-Jones et al. 2018](#)) versus T_{eff} . Error bars are included for both the distances and T_{eff} . The gray solid line at 46.75 pc is the typically quoted distance to the center of the Hyades cluster. The two black horizontal dashed lines delineate the tidal radius of 10 pc for the Hyades; this region is shaded.

of error and the impact of these sources of error on our findings within the Hyades cluster. The rest of the section will be dedicated to a discussion of our findings in the Hyades with respect to the findings of [S2017](#) in the Pleiades. We will also discuss radius inflation as a function of age using these two clusters.

5.1. Potential Sources of Errors

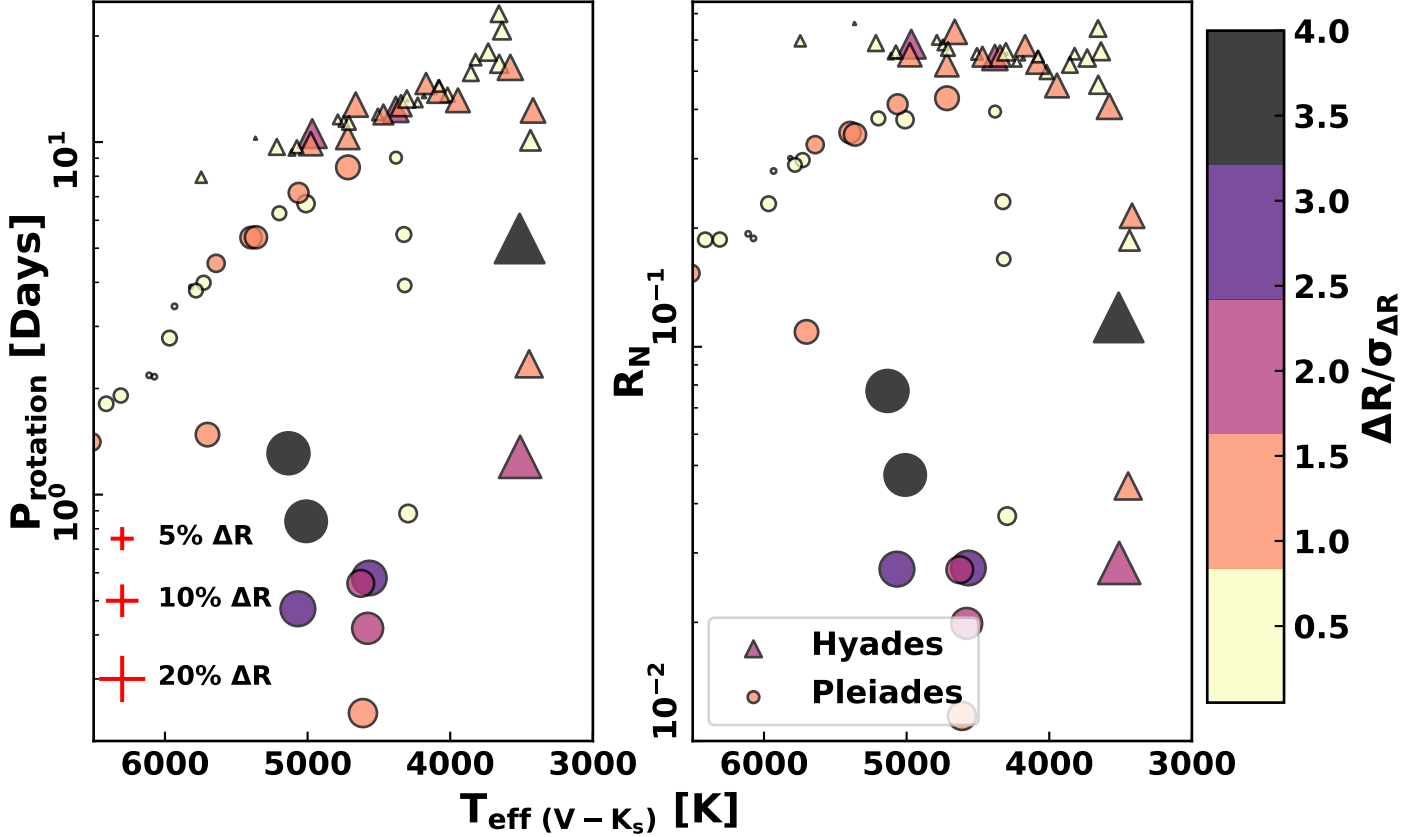


Figure 8. Left plot: Plot of the rotation period and T_{eff} for the Hyades single stars (filled-triangles) and the Pleiades single stars (filled-circles). Right plot: Same as the left plot but now plotting Rossby number (R_N) and T_{eff} . All points within the two panels are sized proportionally to their calculated value of radius inflation (ΔR). The three red crosses in the right panel serve as reference baselines. All points in the two panels are colored according to the sigma significance of the ΔR .

5.1.1. Binaries

As discussed above, binaries are a potential source of false-positive signals of radius inflation since the bolometric flux enhancement from the presence of a secondary would appear as higher luminosity – thus larger radius at fixed temperature – in our analysis. While it is nearly impossible to prove that a star does not have a binary companion, we can assess how efficiently we have excluded binaries by comparing the derived radii of presumed-single and confirmed-binary stars rotating slower than $R_N \sim 0.1$. As these stars are not expected to be inflated by magnetic activity, stars with anomalously large derived radii can be confidently marked as binaries. S2017 did precisely this, finding significantly disparate distributions between the two samples. This provided confidence that most, if not all, binaries had been excluded from the full sample.

We repeat here this same exercise. In the top half of Fig. 6, we plot the periods of single stars with a rotation period greater than 10 days and binaries against their measured radius inflation. In addition to period, we plot the Rossby number (R_N) of the same two sub-samples of stars against their measured radius inflation in the bottom panel of Figure 6. Like S2017, we found that there is a significant contribution

to calculated radius inflation due to binarity. We also found that in considering both rotation period and Rossby number, that the distribution of slowly rotating single stars and binaries are different enough to claim here that we have effectively filtered out binaries from our Hyades sample.

5.1.2. Distance Errors

The calculation of the stellar radius, which is important as the baseline by which a star is judged to be radially inflated or not is vulnerable to either spurious distance measurements or high errors on the distance itself. High error arises from the typical employment of a cluster distance \pm cluster depth, where the cluster depth is then taken as the error on the distance of all the stars. For the Pleiades, this was taken to be 134 ± 3 pc (from Soderblom et al. 2005).

We are able to consider the individual distances to all of our Hyades stars with the *Gaia* DR2 catalog. The *Gaia* DR2 catalog measured proper-motions and parallaxes for over 10^9 stars down to a magnitude limit of $M_G \sim 20$, with parallax errors approaching $40 \mu\text{as}$. For our final sample of Hyades single stars, we found that the *Gaia* DR2 parallax errors span a range of $[37.8, 511.9] \mu\text{as}$ with an average of $86 \mu\text{as}$. Using the distance derivations in parsecs from Bailer-Jones et al. (2018) we have an error on the individual distances of our

single stars spanning the range [0.064, 2.435] pc, with an average distance error of 0.30 pc. We plot the distances and T_{eff} for the single stars in our Hyades sample, along with the relevant errors in Figure 7.

The plotted single stars are all grouped around the typically quoted cluster distance to the Hyades of 46.75 pc (see [Reino et al. 2018](#)). The scatter within this group exhibits the cluster depth along our line of sight and is well within the typically cited tidal radius of the Hyades of ± 10 pc ([Reino et al. 2018](#)). From the Figure 7, as well as the relatively small contribution of distance errors shown in Figure 3, it is apparent that the distance measurements from *Gaia* DR2 for the Hyades are precise enough to employ for our conversion from angular radius to stellar radius.

5.2. Radius Inflation and Cluster Evolution: From the Pleiades to the Hyades

We now have two sets of measurements of radius inflation occurring within open clusters of different ages: The Pleiades cluster which has an estimated age of about 125 Myr and the Hyades cluster which has an estimated age of 625 Myr. With this set of data covering a range of about 500 Myr we now have the opportunity to consider radius inflation in the broader sense of cluster evolution.

One of the aspects that need to be addressed in comparing the Hyades and Pleiades is the inherent mass difference we find between the samples. The Hyades cluster, being about 625 Myr old has spun down considerably more than the Pleiades. We find the effect of this spin down appear as a lower T_{eff} distribution when compared to the younger Pleiades (125 Myr). Our Hyades sample has an average T_{eff} of 4300 K while the Pleiades sample has an average T_{eff} of 5300 K. We test the similarity of these two distributions using the two sample KS test, finding a non-random difference between the two samples. We argue that this does not affect our results as presented, as we are comparing the overall presence of radius inflation as a function of cluster evolution here and not the relative degree of radius inflation.

In the right panel of Fig. 8, we plot the rotation rate of single stars in both the Pleiades (circles) and Hyades (triangles) against their T_{eff} . Each datum is colored according to its inferred radius inflation. As shown before, the stars with convincing evidence of inflation (darkest points) are rotating faster than average for their mass range. However, the inflated Hyades stars rotate slower than the inflated Pleiades stars. In the left panel, we show the same plot with the Rossby number substituted for rotation rate. As low-mass stars have a longer convective overturn timescale, the Rossby numbers of the inflated Hyades are similar to those of the faster-rotating Pleiades. In this panel, the inflated members of both cluster now occupy a similar range, namely $\lesssim 0.2$. That the onset of inflation seems more closely tied to Rossby number than raw rotation rate strongly suggests a link with magnetic properties.

An alternative way to view these data is shown in Figure 9. Here we plot the rotation rate and Rossby number of each star directly against the inferred radius inflation. While there seems to exist a connection between rotation and inflation

in both clusters, in the sense that below a threshold rotation rate stars can show significant inflation, the transition rotation rate does not align for the two clusters. However, in Rossby space we see again an apparent transition around $R_N \sim 0.2$, above which stars cluster around a low ΔR value and above which stars may show large radius inflation values. The most likely explanation for this alignment is that the same magnetic mechanism is operating in both clusters, but sets in at different mass thresholds given the progressive spindown of stars with age.

Many previous studies have considered correlations between Rossby number and the magnetic properties of stars ([Noyes et al. 1984](#); [Pizzolato et al. 2003](#); [Wright et al. 2011](#); [Douglas, et al. 2014](#)). A notable result is that around a Rossby number of 0.1–0.2, there is a break in correlation between rotation rate and magnetic proxies (e.g., $H\alpha$, X-rays, Ca II H&K). Towards larger Rossby numbers, the magnetic proxies decrease in strength with decreasing rotation rate, but at lower Rossby numbers the correlation ceases and the strength of magnetic proxies are approximately constant regardless of the rotation rate. A similar connection between Rossby number and starspot properties has also been noted ([O’dell et al. 1995](#)) SS17 noted that radius inflation set in around this Rossby value in the Pleiades, suggesting a connection. Figure 9 shows that this Rossby threshold appears to hold in the much older Hyades as well, even though the low-Rossby stars are in a different mass range. This strongly suggests that the still-unclear physics of magnetic saturation are related to the onset of radius inflation at high rotation rate.

6. CONCLUSIONS

The causes of radius inflation—the tendency of some low mass stars to be physically larger by $\sim 10\%$ than both theoretical predictions and other stars of equal mass, age, and composition—remains an active area of research. In a recent paper, [S2017](#) searched for the presence of radius inflation among the low mass members of the Pleiades, finding a significant correlation between rapid rotation and radius inflation. This strongly implicated dynamo-generated magnetic fields, which are strong in rapidly-rotating young stars, as the driver of inflation. In this work, we have expanded the reach of this investigation to the older Hyades cluster in order to test how the inflation pattern within clusters evolves as a function of age.

We used archival photometry, distances, and rotation rates for a sample of 68 single-star Hyads between $\sim 0.5 - 1 M_{\odot}$, and empirically determined their T_{eff} s and radii. By assuming a correlation between inflated radius and reduced surface temperature (see §3.6) we calculated the fractional deviation of each star’s radius from theoretical expectations. From this exercise, we found several Hyades members exhibiting radius inflation.

These values reveal a strong correlation between the degree of radius inflation and Rossby number (R_N), a robust indicator of the strength of dynamo-generated magnetic fields. Thus we concluded that Hyades members with R_N below 0.1 (implying very rapid rotation) tend to be physically larger than their siblings with higher R_N s (slower rotation).

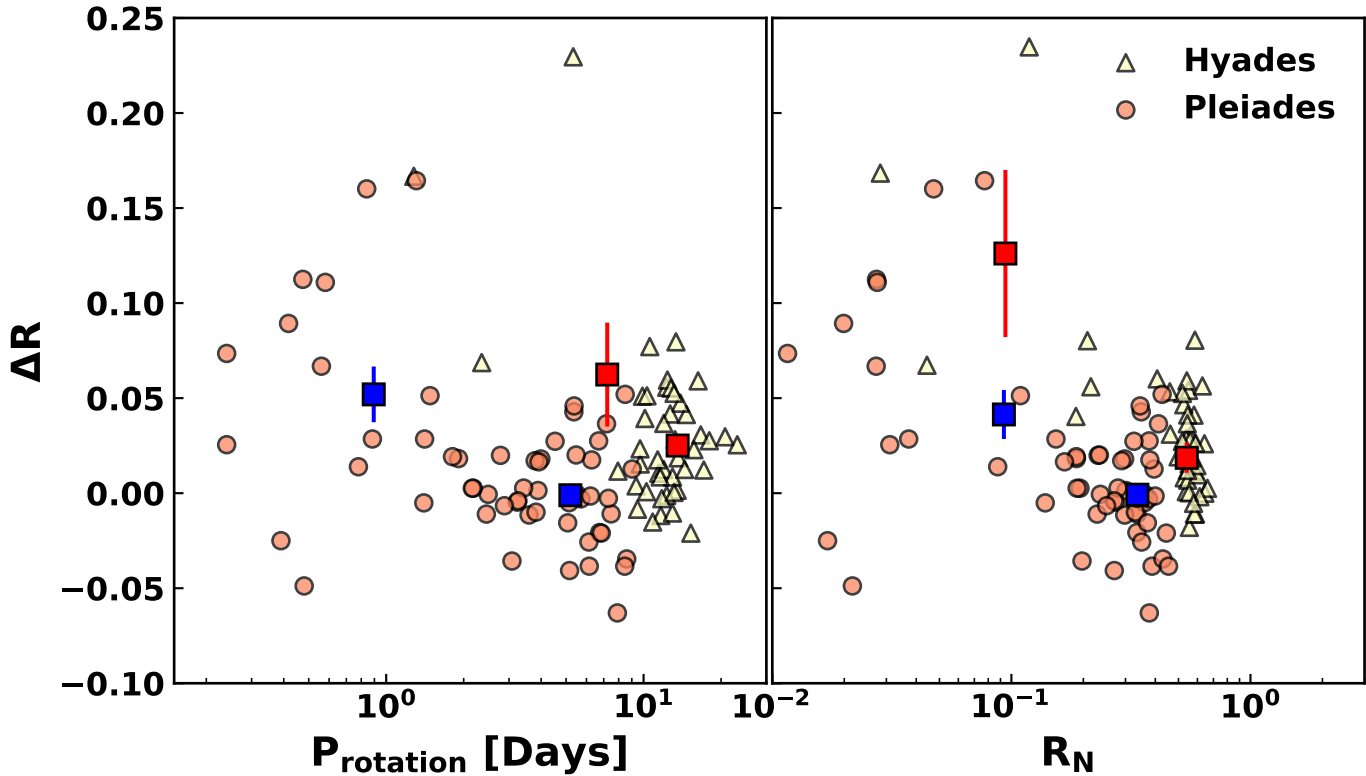


Figure 9. Right Panel: ΔR versus rotation period for both the Pleiades (circles) and Hyades (triangles) samples. The blue and red squares correspond to means of the two bins within the Pleiades and Hyades samples respectively. The Hyades is binned into slow rotators ($P > 10d$) and fast rotators ($P < 10d$). The Pleiades is binned into slow rotators ($P > 2d$) and fast rotators ($P < 2d$). Left panel: Plot of Rossby number (R_N) against ΔR for both the Hyades (triangles) and Pleiades (circles) single star samples. The two red squares are the mean values of ΔR for the rapidly convective ($R_N < 0.2$) and the slowly convective ($R_N > 0.2$) bin of Hyades stars. The blue squares are means for the Pleiades stars, binned the same way.

Finally, we compared these Hyades results to the findings of S2017 for the Pleiades. Those authors only reported a correlation with rotation rate, so we re-analyzed their results with the methods laid out in this paper. We find that the S2017 Pleiades sample also shows a strong correlation between radius inflation and R_N . Moreover, and remarkably, the Pleiades exhibits the same transition point at $R_N \sim 0.1$ as the Hyades, with inflated members below this value and non-inflated members above. This strongly suggests that this R_N threshold for radius inflation is universal, at least over the range of cluster ages spanned by the Pleiades (~ 100 Myr) to the Hyades (~ 700 Myr). Future work should focus on characterizing inflation over a larger range of open cluster ages, in order to assess the full age domain in which this Rossby-inflation correlation persists.

Notably, the mass range of stars with low R_N is lower in the Hyades than in the Pleiades due to the progressive spindown of stars below $\sim 1.3M_\odot$ as they age. This implicates rotation, and not the mass range, as the primary corollary of radius inflation. More fundamentally, because the canoni-

cal rotation-activity relation of low-mass stars is understood to result from the connection between magnetic activity and surface convection, our results imply that magnetic activity within the convective layers of low-mass stars is what preferentially drives radius inflation.

We thank the referee for their comments and suggestions which greatly improved the quality and scope of this paper. KOJ and GS acknowledge the support of the Vanderbilt Office of the Provost through the Vanderbilt Initiative in Data-intensive Astrophysics (VIDA). KOJ thanks the LSSTC Data Science Fellowship Program, which is funded by LSSTC, NSF Cybertraining Grant #1829740, the Brinson Foundation, and the Moore Foundation; their participation in the program has benefited this work. KGS acknowledges NASA grant 17-XRP17 2-0024 for partial support. This research made use of the cross-match service provided by CDS, Strasbourg.

REFERENCES

- Cardelli, J. A., Clayton, G. C., & Mathis, J. S. 1989, *ApJ*, 345, 245
 Chabrier, G., Gallardo, J., & Baraffe, I. 2007, *A&A*, 472, L17
 Chambers, K. C., Magnier, E. A., Metcalfe, N., et al. 2016, arXiv:1612.05560
 Delorme, P., Collier Cameron, A., Hebb, L., et al. 2011, *MNRAS*, 413, 2218
 Douglas S. T., et al., 2014, *ApJ*, 795, 161
 Douglas, S. T., Agüeros, M. A., Covey, K. R., et al. 2016, *ApJ*, 822, 47
 Duchêne, G., Bouvier, J., Moraux, E., et al. 2013, *A&A*, 555, A137
 Fabricius C., Høg E., Makarov V. V., Mason B. D., Wycoff G. L., Urban S. E., 2002, *A&A*, 384, 180
 Feiden, G. A., & Chaboyer, B. 2013, *ApJ*, 779, 183
 Feiden, G. A., & Chaboyer, B. 2014, *ApJ*, 789, 53
 Gaia Collaboration, et al., 2017, *A&A*, 601, A19
 Gaia Collaboration, Brown, A. G. A., Vallenari, A., et al. 2018, *A&A*, 616, A1.
 Goldman, B., Röser, S., Schilbach, E., et al. 2013, *A&A*, 559, A43
 Gunn, J. E., & Stryker, L. L. 1983, *ApJS*, 52, 121
 Huang, Y., Liu, X.-W., Yuan, H.-B., et al. 2015, *MNRAS*, 454, 2863
 Jackson, R. J., & Jeffries, R. D. 2014, *MNRAS*, 441, 2111
 Jackson, R. J., & Jeffries, R. D. 2014, *MNRAS*, 445, 4306
 Jackson, R. J., Jeffries, R. D., Randich, S., et al. 2016, *A&A*, 586, A52
 Jackson, R. J., Deliyannis, C. P., & Jeffries, R. D. 2018, *MNRAS*, 476, 3245
 Johnson, H. L., & Knuckles, C. F. 1955, *ApJ*, 122, 209
 Kopytova, T. G., Brandner, W., Tognelli, E., et al. 2016, *A&A*, 585, A7
 Kurucz, R. L. 2013, *Astrophysics Source Code Library*, ascl:1303.024
 Lawrence, A., Warren, S. J., Almaini, O., et al. 2007, *MNRAS*, 379, 1599
 López-Morales, M., & Ribas, I. 2005, *ApJ*, 631, 1120
 Macdonald, J., & Mullan, D. J. 2010, *ApJ*, 723, 1599
 Martín, E. L., Lodieu, N., Pavlenko, Y., & Béjar, V. J. S. 2018, *ApJ*, 856, 40
 Mason B. D., Wycoff G. L., Hartkopf W. I., Douglass G. G., Worley C. E., 2001, *AJ*, 122, 3466
 Merrelliod J.-C., Mayor M., Udry S., 2009, *A&A*, 498, 949
 Mullan, D. J., & MacDonald, J. 2001, *ApJ*, 559, 353
 Noyes, R. W., Weiss, N. O., & Vaughan, A. H. 1984, *ApJ*, 287, 769
 O'dell, M. A., Panagi, P., Hendry, M. A., & Collier Cameron, A. 1995, *A&A*, 294, 715
 Paulson, D. B., Sneden, C., & Cochran, W. D. 2003, *AJ*, 125, 3185
 Patience, J., Ghez, A. M., Reid, I. N., Weinberger, A. J., & Matthews, K. 1998, *AJ*, 115, 1972
 Pizzoloto, N., Maggio, A., Micela, G., Sciortino, S., & Ventura, P. 2003, *A&A*, 397, 147
 Popper, D. M. 1997, *AJ*, 114, 1195
 Reino, S., de Bruijne, J., Zari, E., d'Antona, F., & Ventura, P. 2018, *MNRAS*, 477, 3197
 Roeser, S., Demleitner, M., & Schilbach, E. 2010, *AJ*, 139, 2440
 Skrutskie, M. F., Cutri, R. M., Stiening, R., et al. 2006, *AJ*, 131, 1163
 Skumanich, A. 1972, *ApJ*, 171, 565
 Soderblom, D. R., Nelan, E., Benedict, G. F., et al. 2005, *AJ*, 129, 1616
 Somers, G., & Pinsonneault, M. H. 2014, *ApJ*, 790, 72
 Somers, G., & Pinsonneault, M. H. 2015, *ApJ*, 807, 174
 Somers, G., & Pinsonneault, M. H. 2015, *MNRAS*, 449, 4131
 Somers, G., & Stassun, K. G. 2017, *AJ*, 153, 101
 Stassun, K. G., Kratter, K. M., Scholz, A., & Dupuy, T. J. 2012, *ApJ*, 756, 47
 Stassun, K. G., & Torres, G. 2016, *AJ*, 152, 180
 Torres, G., & Ribas, I. 2002, *ApJ*, 567, 1140
 Wenger, M., Ochsenein, F., Egret, D., et al. 2000, *A&AS*, 143, 9
 Wright, N. J., Drake, J. J., Mamajek, E. E., & Henry, G. W. 2011, *ApJ*, 743, 48

Table 1. Observed Stellar Properties

2MASS	R.A.	Decl.	Distance (PC)	V_{mag}	$B - V$	$V - K_S$	P_{rot} (Days)	Binary?
03373495+2120355	54.3956	21.3432	45.81 $^{+0.13}_{-0.13}$	9.362±0.008	0.92±0.004	2.240±0.021	10.57	No
03434706+2051363	55.946	20.86	45.21 $^{+0.13}_{-0.13}$	14.54±0.008	0.9±0.004	4.927±0.023	12.3	No
03510309+2354134	57.7628	23.9037	40.83 $^{+0.08}_{-0.08}$	10.118±0.008	1.2819±0.004	2.723±0.021	12.57	Yes
03524101+2548159	58.1708	25.8044	44.41 $^{+0.12}_{-0.12}$	11.21±0.008		3.317±0.027	14.66	No
03550142+1229081	58.7559	12.4855	45.98 $^{+0.09}_{-0.09}$	10.094±0.008	1.07±0.004	2.519±0.022	11.66	No
03583581+1306182	59.6492	13.105	61.24 $^{+0.19}_{-0.19}$	8.951±0.008		1.576±0.022	22.26	Yes?
03590972+2628340	59.7905	26.4761	35.82 $^{+0.09}_{-0.09}$	11.47±0.008		3.585±0.021	15.25	No
03591417+2202380	59.809	22.0439	40.55 $^{+0.08}_{-0.08}$	13.066±0.008		4.362±0.018	20.73	No
04033902+1927180	60.9125	19.455	47.97 $^{+0.11}_{-0.11}$	10.095±0.008	1.08±0.004	2.495±0.021	11.45	No
04052565+1926316	61.3568	19.4421	47.23 $^{+0.12}_{-0.12}$	11.4±0.008	1.35±0.004	3.292±0.027	13.51	No
04063463+1332566	61.6443	13.549	49.84 $^{+0.38}_{-0.38}$	13.409±0.008	1.47±0.004	4.318±0.019	16.68	No
04070122+1520062	61.7551	15.335	45.03 $^{+0.24}_{-0.24}$	10.473±0.008	1.18±0.004	2.808±0.027	11.98	No
04074319+1631076	61.9299	16.5187	46.5 $^{+0.11}_{-0.11}$	9.924±0.008	1.02±0.004	2.412±0.027	12.3	No
04081110+1652229	62.0462	16.873	40.09 $^{+0.07}_{-0.07}$	11.51±0.008	1.44±0.004	3.577±0.025	13.63	No
04082667+1211304	62.1111	12.1918	46.38 $^{+0.15}_{-0.15}$	11.269±0.008	1.33±0.004	3.223±0.028	12.96	No
04083620+2346071	62.1508	23.7686	47.45 $^{+0.13}_{-0.12}$	9.41±0.008	0.9±0.004	2.087±0.016	9.35	No
04084015+2333257	62.1673	23.5571	46.02 $^{+0.17}_{-0.17}$	12.861±0.008		4.332±0.025	21.02	Yes
04115620+2338108	62.9841	23.6363	40.3 $^{+1.19}_{-1.13}$	9.392±0.008		2.982±0.025	2.309	Yes
04151038+1423544	63.7932	14.3984	47.95 $^{+0.09}_{-0.09}$	11.585±0.008	1.38±0.004	3.457±0.018	13.91	No
04153367+1542226	63.8902	15.7062	45.52 $^{+0.14}_{-0.14}$	10.931±0.008		3.077±0.024	47	Yes

Table 1 continued

Table 1 (*continued*)

2MASS	R.A.	Decl.	Distance (PC)	V_{mag}	$B - V$	$V - K_S$	P_{rot} (Days)	Binary?
04163346+2154269	64.1394	21.9074	$51.02^{+0.11}_{-0.11}$	9.125 ± 0.008	0.81 ± 0.004	1.849 ± 0.024	10.26	No
04172512+1901478	64.3547	19.0299	$47.79^{+0.18}_{-0.18}$	10.8 ± 0.008	1.22 ± 0.004	2.891 ± 0.024	12.95	No
04172811+1454038	64.3671	14.901	$49.45^{+0.13}_{-0.13}$	14.47 ± 0.008	1.55 ± 0.004	4.849 ± 0.020	2.35	No
04174767+1339422	64.4486	13.6617	$47.39^{+0.12}_{-0.12}$	12.54 ± 0.008		4.012 ± 0.020	8.685	Yes
04175061+1828307	64.4609	18.4751	$46.65^{+0.31}_{-0.31}$	13.954 ± 0.008		4.962 ± 0.019	22.94	Yes
04175555+1432464	64.4814	14.5462	$52.38^{+0.2}_{-0.2}$	14.89 ± 0.008		4.873 ± 0.018	10.11	No
04181077+2317048	64.5449	23.2846	$53.92^{+0.13}_{-0.13}$	9.471 ± 0.008		2.534 ± 0.017	1.862	Yes
04223953+1816097	65.6647	18.2693	$41.66^{+0.09}_{-0.09}$	13.04 ± 0.008		4.313 ± 0.019	23.12	No
04232283+1939312	65.8451	19.6586	$45.71^{+0.34}_{-0.34}$	9.381 ± 0.008	0.91 ± 0.004	2.230 ± 0.021	9.9	No
04232526+1545474	65.8552	15.7631	$41.47^{+0.15}_{-0.15}$	10.472 ± 0.008	1.24 ± 0.004	2.977 ± 0.019	12.38	No
04235070+0912193	65.9612	9.20538	$44.83^{+0.11}_{-0.11}$	12.896 ± 0.008	1.51 ± 0.004	4.67 ± 0.019	5.33	No
04235911+1643178	65.9963	16.7216	$46.0^{+0.12}_{-0.12}$	12.514 ± 0.008	1.49 ± 0.004	3.952 ± 0.019	17.14	No
04241691+1800107	66.0704	18.0029	$46.66^{+0.09}_{-0.09}$	9.966 ± 0.008	1.06 ± 0.004	2.441 ± 0.019	11.6	No
04250024+1659057	66.251	16.9849	$54.61^{+0.19}_{-0.19}$	10.248 ± 0.008	1.03 ± 0.004	2.417 ± 0.017	11.77	No
04251456+1858250	66.3106	18.9736	$52.87^{+0.2}_{-0.2}$	12.728 ± 0.008	1.48 ± 0.004	4.022 ± 0.019	10.84	Yes
04252501+1754552	66.3542	17.9153	$46.85^{+0.09}_{-0.09}$	11.128 ± 0.008		3.151 ± 0.019	70	Yes
04254754+1801022	66.448	18.0172	$42.11^{+1.05}_{-1.0}$	8.9889 ± 0.008	0.94 ± 0.004	2.221 ± 0.022	8.46	Yes
04264825+1052160	66.701	10.8711	$46.97^{+1.01}_{-0.97}$	9.432 ± 0.008	1.04 ± 0.004	2.549 ± 0.021	10.4	Yes
04272532+1415384	66.8555	14.2606	$52.59^{+0.51}_{-0.5}$	10.313 ± 0.008	1.08 ± 0.004	2.600 ± 0.024	12.77	No
04274701+1425041	66.9459	14.4178	$49.32^{+0.1}_{-0.1}$	9.475 ± 0.008	0.92 ± 0.004	2.127 ± 0.021	9.7	No
04275895+1830009	66.9956	18.5002	$51.06^{+0.27}_{-0.27}$	10.129 ± 0.008		2.596 ± 0.019	11.13	Yes
04282878+1741453	67.1199	17.6959	$46.83^{+0.58}_{-0.57}$	12.122 ± 0.008	1.49 ± 0.004	4.411 ± 0.027	2.42	Yes
04303385+1444532	67.641	14.7481	$49.98^{+1.17}_{-1.12}$	14.72 ± 0.008	1.56 ± 0.004	5.008 ± 0.019	18.41	Yes
04303486+1544023	67.6452	15.7339	$57.07^{+0.9}_{-0.87}$	8.84 ± 0.008	0.84 ± 0.004	2.022 ± 0.019	8.73	Yes
04315244+1529585	67.9685	15.4995	$45.73^{+0.08}_{-0.08}$	11.0 ± 0.008	1.31 ± 0.004	3.105 ± 0.025	13.13	No
04322565+1306476	68.1068	13.1132	$46.72^{+0.1}_{-0.1}$	11.0 ± 0.008	1.19 ± 0.004	3.346 ± 0.021	1.48	Yes
04332699+1302438	68.3624	13.0455	$43.09^{+0.1}_{-0.1}$	13.328 ± 0.008	1.57 ± 0.004	4.505 ± 0.020	16.29	No
04333716+2109030	68.4048	21.1508	$43.74^{+0.09}_{-0.09}$	10.726 ± 0.008	1.23 ± 0.004	3.040 ± 0.027	12.69	No
04341113+1133285	68.5464	11.5579	$47.78^{+0.5}_{-0.49}$	11.25 ± 0.008	1.39 ± 0.004	3.191 ± 0.030	11.03	Yes
04354850+1317169	68.9521	13.288	$49.17^{+0.14}_{-0.14}$	14.91 ± 0.008	1.63 ± 0.004	5.042 ± 0.019	13.36	No
04360525+1541026	69.0218	15.684	$50.15^{+0.12}_{-0.12}$	9.345 ± 0.008	0.87 ± 0.004	1.972 ± 0.016	9.47	No
04395095+1243426	69.9623	12.7285	$43.63^{+0.09}_{-0.09}$	9.992 ± 0.008	1.07 ± 0.004	2.512 ± 0.024	10.85	No
04412780+1404340	70.3658	14.0761	$49.2^{+1.28}_{-1.22}$	13.395 ± 0.008		4.683 ± 0.022	1.28	No
04412876+1200337	70.3698	12.0093	$47.16^{+0.1}_{-0.09}$	12.898 ± 0.008	1.5 ± 0.004	4.144 ± 0.021	18	No
04431568+1704088	70.8153	17.0691	$45.88^{+0.41}_{-0.4}$	9.92 ± 0.008	1.0 ± 0.004	2.524 ± 0.017	10.31	No
04461879+0338108	71.5783	3.63636	$45.1^{+0.08}_{-0.08}$	10.922 ± 0.008	1.27 ± 0.004	3.096 ± 0.021	13.25	No
04463036+1528194	71.6265	15.472	$49.05^{+0.21}_{-0.2}$	8.28 ± 0.008	0.66 ± 0.004	1.541 ± 0.033	7.95	No
04471851+0627113	71.8271	6.45315	$40.54^{+0.07}_{-0.06}$	11.348 ± 0.008	1.42 ± 0.004	3.473 ± 0.027	14.44	No
04480086+1703216	72.0036	17.056	$44.13^{+0.9}_{-0.87}$	11.085 ± 0.008	1.41 ± 0.004	3.711 ± 0.024	10.77	Yes
04483062+1623187	72.1276	16.3885	$48.12^{+0.13}_{-0.13}$	12.427 ± 0.008	1.47 ± 0.004	3.884 ± 0.018	15.69	No
04484211+2106035	72.1754	21.1009	$45.37^{+0.23}_{-0.23}$	9.057 ± 0.008	0.85 ± 0.004	1.985 ± 0.019	9.69	No
04491296+2448103	72.304	24.8028	$49.59^{+0.14}_{-0.14}$	9.492 ± 0.008	1.04 ± 0.004	2.536 ± 0.038	6.9	Yes
04500069+1624436	72.5028	16.4121	$49.34^{+0.13}_{-0.13}$	10.69 ± 0.008	1.16 ± 0.004	2.851 ± 0.017	11.98	No
04510241+1458167	72.76	14.9713	$40.77^{+0.75}_{-0.72}$	11.675 ± 0.008		3.708 ± 0.021	13.14	No
04522352+1859489	73.098	18.9969	$50.75^{+0.12}_{-0.12}$	10.28 ± 0.008	1.07 ± 0.004	2.537 ± 0.021	11.34	No
04522385+1043099	73.0994	10.7194	$52.04^{+0.14}_{-0.14}$	12.816 ± 0.008		4.044 ± 0.023	9.88	Yes?

Table 1 *continued*

Table 1 (*continued*)

2MASS	R.A.	Decl.	Distance (PC)	V_{mag}	$B - V$	$V - K_S$	P_{rot} (Days)	Binary?
05054038+0627545	76.4182	6.46515	$65.44^{+1.43}_{-1.37}$	9.88 ± 0.008	0.95 ± 0.004	2.362 ± 0.022	10.41	Yes
05110971+1548574	77.7904	15.8159	$57.09^{+2.44}_{-2.25}$	12.08 ± 0.008		3.977 ± 0.018	14.94	Yes?

Table 2. Derived Stellar Properties ($V - K_s$)

2MASS	T_{eff} (K)	σ_{teff} (Systematic) (K)	\mathcal{F}_{bol} $\times 10^{-10}$ ($\text{erg cm}^{-2} \text{s}^{-1}$)	χ^2_{ν}	Angular Diameter $\times 10^{-2}$ (mas)	Radius (R_{\odot})	Δ Radius (%)
3373495+2120355	4967 ± 14.29	60	$62.8^{+2.0}_{-2.52}$	1.22	$8.8^{+0.15}_{-0.18}$	$0.87^{+0.01}_{-0.02}$	$7.7108^{+3.663}_{-3.663}$
3434706+2051363	3419 ± 6.36	60	$2.67^{+0.245}_{-0.215}$	7.21	$3.83^{+0.18}_{-0.15}$	$0.37^{+0.02}_{-0.02}$	$5.5743^{+6.351}_{-6.351}$
3510309+2354134	4565 ± 11.71	60	$36.5^{+1.3599}_{-0.975}$	2.8	$7.94^{+0.15}_{-0.11}$	$0.7^{+0.01}_{-0.01}$	$-0.044^{+3.655}_{-3.655}$
3524101+2548159	4169 ± 12.35	60	$19.6^{+0.571}_{-0.547}$	0.95	$6.98^{+0.11}_{-0.11}$	$0.67^{+0.01}_{-0.01}$	$4.1394^{+3.929}_{-3.929}$
3550142+1229081	4725 ± 13.34	60	$34.5^{+1.97}_{-1.820}$	5.98	$7.2^{+0.21}_{-0.19}$	$0.71^{+0.02}_{-0.02}$	$-1.172^{+4.171}_{-4.171}$
3583581+1306182	5686 ± 20.52	60	$71.5^{+3.6400}_{-3.39}$	6.11	$7.16^{+0.19}_{-0.18}$	$0.94^{+0.03}_{-0.02}$	$-0.048^{+3.818}_{-3.818}$
3590972+2628340	4012 ± 8.59	60	$18.2^{+0.364}_{-0.527}$	1.18	$7.26^{+0.08}_{-0.11}$	$0.56^{+0.01}_{-0.01}$	$-2.101^{+3.496}_{-3.496}$
3591417+2202380	3637 ± 5.89	60	$7.090^{+0.4479}_{-0.458}$	8.71	$5.51^{+0.18}_{-0.18}$	$0.48^{+0.02}_{-0.02}$	$2.9676^{+4.954}_{-4.954}$
4033902+1927180	4745 ± 12.84	60	$34.9^{+1.66}_{-1.55}$	2.5	$7.19^{+0.18}_{-0.16}$	$0.74^{+0.02}_{-0.02}$	$1.0510^{+3.930}_{-3.930}$
4052565+1926316	4183 ± 12.45	60	$15.5^{+0.552}_{-0.524}$	2.04	$6.16^{+0.12}_{-0.11}$	$0.63^{+0.01}_{-0.01}$	$0.1523^{+3.908}_{-3.908}$
04063463+1332566	3656 ± 6.25	60	$5.020^{+0.29}_{-0.303}$	6.28	$4.59^{+0.13}_{-0.14}$	$0.49^{+0.01}_{-0.02}$	$3.0635^{+4.840}_{-4.840}$
04070122+1520062	4506 ± 14.91	60	$28.80^{+0.8029}_{-0.771}$	0.49	$7.24^{+0.11}_{-0.11}$	$0.7^{+0.01}_{-0.01}$	$1.2427^{+3.690}_{-3.690}$
04074319+1631076	4819 ± 17.5	60	$39.5^{+1.44}_{-1.69}$	5.32	$7.41^{+0.15}_{-0.17}$	$0.74^{+0.01}_{-0.02}$	$-0.111^{+3.700}_{-3.700}$
04081110+1652229	4018 ± 10.36	60	$17.1^{+0.8260}_{-0.917}$	5.33	$7.01^{+0.17}_{-0.19}$	$0.61^{+0.01}_{-0.02}$	$1.8593^{+4.336}_{-4.336}$
04082667+1211304	4227 ± 13.31	60	$17.7^{+0.33}_{-0.162}$	0.29	$6.45^{+0.07}_{-0.05}$	$0.64^{+0.01}_{-0.01}$	$0.8483^{+3.636}_{-3.636}$
04083620+2346071	5109 ± 11.96	60	$55.89^{+1.56}_{-1.49}$	1.55	$7.84^{+0.12}_{-0.11}$	$0.8^{+0.01}_{-0.01}$	$0.3837^{+3.166}_{-3.166}$
04084015+2333257	3652 ± 8.17	60	$8.68^{+0.534}_{-0.489}$	4.8	$6.05^{+0.19}_{-0.17}$	$0.6^{+0.02}_{-0.02}$	$11.581^{+5.412}_{-5.412}$
04115620+2338108	4381 ± 12.79	60	$88.1^{+2.73}_{-3.87}$	2.85	$13.39^{+0.22}_{-0.3}$	$1.16^{+0.04}_{-0.04}$	$41.846^{+6.679}_{-6.679}$
04151038+1423544	4081 ± 7.75	60	$14.80^{+0.669}_{-0.381}$	2.83	$6.32^{+0.14}_{-0.08}$	$0.65^{+0.02}_{-0.01}$	$4.7336^{+4.210}_{-4.210}$
04153367+1542226	4317 ± 11.8	60	$21.29^{+1.16}_{-1.08}$	7.22	$6.78^{+0.19}_{-0.18}$	$0.66^{+0.02}_{-0.02}$	$1.0256^{+4.354}_{-4.354}$
04163346+2154269	5365 ± 19.71	60	$66.8^{+1.29}_{-2.46}$	4.05	$7.78^{+0.09}_{-0.15}$	$0.85^{+0.01}_{-0.02}$	$0.0777^{+3.134}_{-3.134}$
04172512+1901478	4445 ± 12.66	60	$21.8^{+0.9770}_{-0.915}$	6.27	$6.47^{+0.15}_{-0.14}$	$0.67^{+0.02}_{-0.01}$	$-1.043^{+3.939}_{-3.939}$
04172811+1454038	3446 ± 5.68	60	$2.900^{+0.154}_{-0.123}$	4.14	$3.93^{+0.11}_{-0.08}$	$0.42^{+0.01}_{-0.01}$	$6.8703^{+4.971}_{-4.971}$
04174767+1339422	3794 ± 7.16	60	$8.690^{+0.581}_{-0.528}$	8.58	$5.61^{+0.19}_{-0.17}$	$0.57^{+0.02}_{-0.02}$	$4.8220^{+5.110}_{-5.110}$
04175061+1828307	3405 ± 5.28	60	$4.979^{+0.287}_{-0.264}$	5.82	$5.27^{+0.15}_{-0.14}$	$0.53^{+0.02}_{-0.01}$	$16.098^{+5.621}_{-5.621}$
04175555+1432464	3437 ± 5.16	60	$1.870^{+0.1750}_{-0.037}$	7.03	$3.17^{+0.15}_{-0.03}$	$0.36^{+0.02}_{-0.0}$	$3.9298^{+6.272}_{-6.272}$
04181077+2317048	4710 ± 10.37	60	$66.1^{+2.06}_{-1.97}$	0.81	$10.04^{+0.16}_{-0.16}$	$1.17^{+0.02}_{-0.02}$	$33.526^{+4.510}_{-4.510}$
04223953+1816097	3658 ± 6.26	60	$7.02^{+0.3}_{-0.282}$	3.41	$5.42^{+0.12}_{-0.11}$	$0.49^{+0.01}_{-0.01}$	$2.5476^{+4.319}_{-4.319}$
04232283+1939312	4977 ± 14.36	60	$59.0^{+2.0100}_{-3.13}$	8.35	$8.49^{+0.15}_{-0.23}$	$0.84^{+0.02}_{-0.02}$	$5.1025^{+3.700}_{-3.700}$
04232526+1545474	4381 ± 9.63	60	$32.8^{+0.6310}_{-0.912}$	0.6	$8.17^{+0.09}_{-0.12}$	$0.73^{+0.01}_{-0.01}$	$5.9528^{+3.538}_{-3.538}$
04235070+0912193	3513 ± 5.68	60	$9.959^{+0.7859}_{-0.591}$	8.15	$7.0^{+0.28}_{-0.21}$	$0.68^{+0.03}_{-0.02}$	$22.958^{+6.690}_{-6.690}$
04235911+1643178	3822 ± 6.95	60	$8.42^{+0.66}_{-0.591}$	5.06	$5.44^{+0.21}_{-0.19}$	$0.54^{+0.02}_{-0.02}$	$1.2178^{+5.327}_{-5.327}$
04241691+1800107	4788 ± 11.88	60	$38.8^{+0.6990}_{-0.679}$	0.65	$7.44^{+0.08}_{-0.07}$	$0.75^{+0.01}_{-0.01}$	$0.8544^{+3.168}_{-3.168}$
04250024+1659057	4806 ± 10.87	60	$28.00^{+1.01}_{-0.954}$	1.91	$6.27^{+0.12}_{-0.11}$	$0.74^{+0.01}_{-0.01}$	$-0.287^{+3.463}_{-3.463}$
04251456+1858250	3789 ± 6.81	60	$7.25^{+0.54}_{-0.485}$	4.89	$5.14^{+0.19}_{-0.17}$	$0.58^{+0.02}_{-0.02}$	$6.0036^{+5.451}_{-5.451}$

Table 2 *continued*

Table 2 (continued)

2MASS	T_{eff} (K)	σ_{teff} (Systematic) (K)	\mathcal{F}_{bol} $\times 10^{-10}$ (erg cm $^{-2}$ s $^{-1}$)	χ^2_{ν}	Angular Diameter $\times 10^{-2}$ (mas)	Radius (R_{\odot})	Δ Radius (%)
04252501+1754552	4267±9.04	60	17.9 $^{+0.9440}_{-1.01}$	8.25	6.36 $^{+0.17}_{-0.18}$	0.64 $^{+0.02}_{-0.02}$	-0.111 $^{+4.173}_{-4.173}$
04254754+1801022	4985±15.13	60	86.2 $^{+3.0900}_{-4.8}$	3.69	10.23 $^{+0.19}_{-0.29}$	0.93 $^{+0.03}_{-0.03}$	11.693 $^{+4.799}_{-4.799}$
04264825+1052160	4700±12.55	60	67.1 $^{+1.63}_{-3.82}$	6.11	10.16 $^{+0.13}_{-0.29}$	1.03 $^{+0.03}_{-0.04}$	24.501 $^{+4.923}_{-4.923}$
04272532+1415384	4662±14.19	60	29.8 $^{+0.532}_{-0.518}$	0.91	6.88 $^{+0.07}_{-0.07}$	0.78 $^{+0.01}_{-0.01}$	5.5282 $^{+3.632}_{-3.632}$
04274701+1425041	5075±15.03	60	51.4 $^{+0.9609}_{-1.39}$	2.81	7.62 $^{+0.08}_{-0.11}$	0.81 $^{+0.01}_{-0.01}$	1.5360 $^{+3.155}_{-3.155}$
04275895+1830009	4662±11.16	60	35.8 $^{+1.06}_{-1.02}$	2.62	7.54 $^{+0.12}_{-0.11}$	0.83 $^{+0.01}_{-0.01}$	9.7850 $^{+3.769}_{-3.769}$
04282878+1741453	3620±8.69	60	16.9 $^{+1.0}_{-0.920}$	5.68	8.59 $^{+0.26}_{-0.24}$	0.87 $^{+0.03}_{-0.03}$	36.433 $^{+6.779}_{-6.779}$
04303385+1444532	3389±5.22	60	2.59 $^{+0.134}_{-0.124}$	4.94	3.84 $^{+0.1}_{-0.09}$	0.41 $^{+0.01}_{-0.01}$	9.2007 $^{+5.673}_{-5.673}$
04303486+1544023	5176±14.26	60	87.4 $^{+3.15}_{-2.99}$	8.41	9.56 $^{+0.18}_{-0.17}$	1.17 $^{+0.03}_{-0.03}$	22.461 $^{+4.575}_{-4.575}$
04315244+1529585	4300±12.22	60	19.9 $^{+0.771}_{-0.904}$	8.11	6.61 $^{+0.13}_{-0.15}$	0.65 $^{+0.01}_{-0.02}$	0.0410 $^{+3.882}_{-3.882}$
04322565+1306476	4148±9.31	60	22.9 $^{+1.5}_{-1.150}$	5.87	7.62 $^{+0.25}_{-0.19}$	0.77 $^{+0.03}_{-0.02}$	13.762 $^{+5.328}_{-5.328}$
04332699+1302438	3578±6.21	60	6.11 $^{+0.3500}_{-0.322}$	5.88	5.29 $^{+0.15}_{-0.14}$	0.49 $^{+0.01}_{-0.01}$	5.9090 $^{+4.961}_{-4.961}$
04333716+2109030	4344±13.65	60	26.5 $^{+0.758}_{-0.962}$	2.3	7.47 $^{+0.12}_{-0.14}$	0.7 $^{+0.01}_{-0.01}$	4.1654 $^{+3.839}_{-3.839}$
04341113+1133285	4248±14.58	60	17.80 $^{+0.7159}_{-0.838}$	1.99	6.4 $^{+0.14}_{-0.16}$	0.66 $^{+0.02}_{-0.02}$	1.7683 $^{+4.250}_{-4.250}$
04354850+1317169	3377±nan	60	2.199 $^{+0.147}_{-0.133}$	6.86	3.56 $^{+nan}_{-nan}$	0.38 $^{+nan}_{-nan}$	7.9629 $^{+nan}_{-nan}$
04360525+1541026	5225±12.6	60	55.79 $^{+1.05}_{-2.02}$	4.13	7.49 $^{+0.08}_{-0.14}$	0.81 $^{+0.01}_{-0.02}$	-0.844 $^{+2.918}_{-2.918}$
04395095+1243426	4733±14.7	60	38.3 $^{+0.684}_{-0.993}$	3.26	7.56 $^{+0.08}_{-0.11}$	0.71 $^{+0.01}_{-0.01}$	-1.518 $^{+3.237}_{-3.237}$
04412780+1404340	3509±6.49	60	6.42 $^{+0.4870}_{-0.437}$	4.78	5.63 $^{+0.21}_{-0.19}$	0.6 $^{+0.03}_{-0.03}$	16.672 $^{+6.953}_{-6.953}$
04412876+1200337	3733±7.21	60	6.88 $^{+0.468}_{-0.425}$	9.4	5.15 $^{+0.18}_{-0.16}$	0.52 $^{+0.02}_{-0.02}$	2.7593 $^{+5.093}_{-5.093}$
04431568+1704088	4718±10.41	60	41.7 $^{+2.59}_{-1.609}$	2.13	7.95 $^{+0.25}_{-0.16}$	0.78 $^{+0.03}_{-0.02}$	5.1217 $^{+4.621}_{-4.621}$
04461879+0338108	4303±10.17	60	22.5 $^{+0.634}_{-0.408}$	0.55	7.01 $^{+0.1}_{-0.07}$	0.68 $^{+0.01}_{-0.01}$	2.8151 $^{+3.657}_{-3.657}$
04463036+1528194	5745±34.28	60	127.0 $^{+5.5100}_{-1.32}$	1.61	9.35 $^{+0.23}_{-0.12}$	0.99 $^{+0.02}_{-0.01}$	1.1597 $^{+4.002}_{-4.002}$
04471851+0627113	4077±11.7	60	18.2 $^{+1.12}_{-1.02}$	5.98	7.03 $^{+0.22}_{-0.2}$	0.61 $^{+0.02}_{-0.02}$	1.2485 $^{+4.733}_{-4.733}$
04480086+1703216	3946±9.48	60	26.0 $^{+1.89}_{-1.71}$	6.7	8.97 $^{+0.33}_{-0.3}$	0.85 $^{+0.04}_{-0.03}$	26.207 $^{+6.890}_{-6.890}$
04483062+1623187	3855±6.77	60	8.709 $^{+0.7509}_{-0.727}$	5.15	5.44 $^{+0.24}_{-0.23}$	0.56 $^{+0.02}_{-0.02}$	2.2890 $^{+5.663}_{-5.663}$
04484211+2106035	5215±14.51	60	74.9 $^{+2.98}_{-4.82}$	5.97	8.71 $^{+0.18}_{-0.28}$	0.85 $^{+0.02}_{-0.03}$	2.3311 $^{+3.602}_{-3.602}$
04491296+2448103	4726±25.52	60	60.6 $^{+2.37}_{-2.96}$	2.95	9.55 $^{+0.21}_{-0.25}$	1.02 $^{+0.02}_{-0.03}$	23.383 $^{+5.086}_{-5.086}$
04500069+1624436	4468±9.16	60	24.5 $^{+1.38}_{-1.27}$	4.67	6.79 $^{+0.19}_{-0.18}$	0.72 $^{+0.02}_{-0.02}$	3.6727 $^{+4.347}_{-4.347}$
04510241+1458167	3945±8.25	60	16.3 $^{+0.655}_{-0.617}$	2.0	7.1 $^{+0.15}_{-0.14}$	0.62 $^{+0.02}_{-0.02}$	5.2541 $^{+4.629}_{-4.629}$
04522352+1859489	4710±12.61	60	30.4 $^{+1.2200}_{-1.150}$	2.89	6.81 $^{+0.14}_{-0.13}$	0.74 $^{+0.02}_{-0.01}$	1.7520 $^{+3.751}_{-3.751}$
04522385+1043099	3780±8.15	60	7.040 $^{+0.368}_{-0.406}$	2.92	5.08 $^{+0.13}_{-0.15}$	0.57 $^{+0.02}_{-0.02}$	5.0041 $^{+4.684}_{-4.684}$
05054038+0627545	4859±14.25	60	41.7 $^{+0.4100}_{-0.404}$	0.26	7.49 $^{+0.06}_{-0.06}$	1.06 $^{+0.02}_{-0.02}$	22.910 $^{+4.659}_{-4.659}$
05110971+1548574	3809±6.58	60	13.69 $^{+0.3629}_{-0.349}$	1.35	6.99 $^{+0.1}_{-0.09}$	0.86 $^{+0.04}_{-0.04}$	30.224 $^{+7.385}_{-7.385}$